

# Non-Hermitian Aharonov-Bohm Cage

S. M. Zhang and L. Jin\*

*School of Physics, Nankai University, Tianjin 300071, China*

Aharonov-Bohm (AB) cage has a spectrum fully constituted by the flat bands and has the capacity to confine arbitrary excitation. The confined excitation in coupled waveguides propagates without diffraction. Exploited the unidirectionality of the exceptional point (EP), we first propose the non-Hermitian AB cage in the photonic crystal with inversion symmetry or combined-inversion symmetry. Alternatively, the destructive interference of the synthetic magnetic flux incorporated with gain and loss at the EP is then shown to be able to induce the non-Hermitian AB cage. The spectrum of the non-Hermitian AB cage is entirely constituted by the coalesced flat bands. The light excitation is still confined regardless of the nonunitary dynamics caused by the non-Hermiticity, but the localization area may alter. The non-Hermitian AB caging can also be observed in the passive photonic crystals including coupled waveguides. These findings pave the way of light control and manipulation in the non-Hermitian integrated photonics.

*Introduction.*—Light flow engineering is fundamentally important in optics. The confinement of light is an important task for light control and manipulation. The flat bands are dispersiveless, support the compact localized state (CLS), and play a pivotal role for the light confinement. A vast of one-dimensional (1D) and two-dimensional (2D) lattices support flat bands [1–11] and have been demonstrated experimentally in the direct femtosecond laser writing of optical waveguides [12–16]. In addition, the photonic system serves as an ideal platform for the study of non-Hermitian physics [17–24]. Flat bands in non-Hermitian photonic crystals are successfully proposed [25–32]. The  $\mathcal{PT}$ -symmetric real-energy flat band is observed at the band gap closure of a non-Hermitian triangular coupled waveguide lattice [27, 28].

In contrast to the general confinement of flat-band CLS, an Aharonov-Bohm (AB) cage completely confines the light excitation that is not limited to the CLS of the system. This is a consequence that the spectrum of AB cage is fully consisted of flat bands [33, 34]. Recently, a rhombic lattice with a half quantum magnetic flux in each plaquette forms an AB cage and has been realized experimentally in the coupled waveguides [35–39]. Here, we exploit the exceptional point (EP) to propose non-Hermitian AB cages in the 1D and 2D photonic resonator lattices, where all the bands are flat and consisting of coalesced energy levels. The oppositely orientated unidirectional couplings or the destructive interference at the proper match between synthetic magnetic flux and balanced gain and loss at the EP induces the non-Hermitian AB caging. Although the band energies are entirely real and arbitrary excitation is completely confined, the excitation intensities in the non-Hermitian AB cages can be constant, oscillate or polynomially increase with time and the localization area of excitation may alter.

*Confinement by unidirectional coupling.*—The EP provides many potential applications [24] including optical sensing [40–51], power transfer [52, 53], and unidirectional lasing [54–56]. The perfect unidirectionality is an intrinsic feature of the EP. The nonreciprocal (asymmet-

ric) coupling strength results in one-way amplification or attenuation; an extreme case is the unidirectional coupling at the EP, where tunneling is one-way allowed and photons in one site can tunnel to the other site with the prohibition of the reverse process. This inspires the design of non-Hermitian AB cages as a novel application of the EP for the complete light confinement by alternatively introducing the unidirectional couplings. Arbitrary light excitation will be confined inside the area with only inward unidirectional couplings connected to the outside.

In Hermitian optical structures, the nonreciprocity can be generated through dynamical modulation [57], optomechanical coupling [58], or optical nonlinearity in asymmetric systems [59]. In non-Hermitian optical structures, the gain and loss associated with synthetic magnetic flux create the nonreciprocity [56]. The external pumping induces gain [60–62]; intentionally introduced absorption induces loss. For example, fabricating the radiative loss [63–65] or cutting the waveguide [66] generates extra loss in coupled waveguides; while sticking additional material with strong absorption generates extra loss in coupled resonators [63]. Besides, the asymmetric coupling has been proposed in coupled resonator array by imposing an effective imaginary magnetic field [67]. Both approaches enable the nonreciprocity and optical diode in non-Hermitian metamaterial [68].

*Unidirectional coupling induced AB cage.*—In Fig. 1(a), all the primary resonators (round shape) have resonant frequency  $\omega_c$ , evanescently coupled to the auxiliary resonators (stadium shape). The auxiliary resonators with black arrows induce reciprocal (symmetric) couplings between the primary resonators [69] and the auxiliary resonators with colored arrows induce asymmetric couplings [67]. In the coupled ring resonator array, extra gain and loss present in the half-perimeter of the auxiliary resonators. Photons tunneling between the primary resonators through the auxiliary resonators are amplified or attenuated and the effective coupling strength induced between the primary resonators is

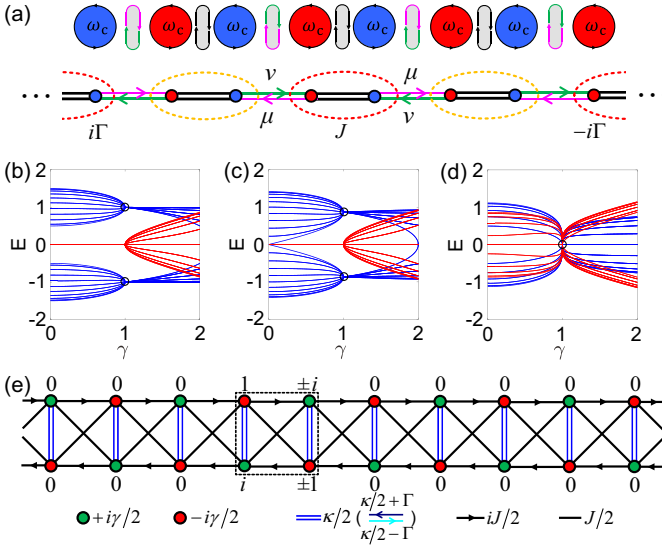


FIG. 1. (a) Schematic of the 1D non-Hermitian coupled resonator array, which is inversion symmetric (chiral-inversion symmetric) when  $\Gamma = 0$  ( $\Gamma \neq 0$ ). Spectra of (a) at (b)  $\Gamma = 0$ , (c)  $\Gamma = 1/2$ , and (d)  $\Gamma = 1$  with the real (imaginary) part in blue (red); the zero energy corresponds to  $\omega_c$ . Non-Hermitian AB caging with all bands flat at energy  $\pm 1$ ,  $\pm\sqrt{3}/2$ , and 0 occurs at the EP  $\mu = 0$  when  $\gamma = 1$ . Other parameters are  $J = \kappa = 1$ , and the lattice size is 40. (e) Schematic of the quasi-1D non-Hermitian cross-stitch lattice. Each plaquette has a  $\pi$  synthetic magnetic flux. The pair of CLSs is localized in a single unit cell at  $\gamma = \kappa$ . Asymmetric couplings  $\kappa/2 + \Gamma$  in the bracket are downward for  $\Gamma \neq 0$ .

tunneling direction dependent [67]; consequently, extra half-perimeter gain (loss) in the auxiliary resonator leads to the asymmetric coupling and creates an imaginary gauge field [70–73].

The equations of motion for the light field of the resonator array in the coupled mode theory is equivalent to the discrete Schrödinger equations for the 1D lattice shown in the lower panel of Fig. 1(a) [13, 27, 56, 74]; the Hamiltonian of the schematic lattice models the resonator array. In coupled mode theory, the equations of motion for the light field in the chiral-inversion symmetric non-Hermitian photonic crystal lattice for the nonzero  $\Gamma$  are in the following form

$$i \frac{d\varphi_{4j}}{dt} = -i\Gamma\varphi_{4j} + \nu\varphi_{4j-1} + J\varphi_{4j+1}, \quad (1)$$

$$i \frac{d\varphi_{4j+1}}{dt} = i\Gamma\varphi_{4j+1} + J\varphi_{4j} + \nu\varphi_{4j+2}, \quad (2)$$

$$i \frac{d\varphi_{4j+2}}{dt} = -i\Gamma\varphi_{4j+2} + \mu\varphi_{4j+1} + J\varphi_{4j+3}, \quad (3)$$

$$i \frac{d\varphi_{4j+3}}{dt} = i\Gamma\varphi_{4j+3} + J\varphi_{4j+2} + \mu\varphi_{4j+4}, \quad (4)$$

which are equivalent to the discrete Schrödinger equations of a 1D non-Hermitian lattice Hamiltonian  $H$  and  $\varphi_l$  is the light field amplitude (wave function) in the  $l$ -th primary resonator. The subscript  $l$  is the index of the

lattice from the left to the right of Fig. 1(a). The equations of motion also describe the dynamics of the coupled waveguide lattice.

The non-Hermitian Aharonov-Bohm (AB) cage forms at the exceptional point (EP) of the 1D non-Hermitian lattice, which is also  $\mathcal{PT}$ -symmetric and the EP is the  $\mathcal{PT}$ -symmetric phase transition point. The Hamiltonian of the 1D non-Hermitian lattice at the EP is unable to be diagonalized. However, the time evolution dynamics of the non-Hermitian AB cage can be straightforwardly obtained from solving the discrete Schrödinger equations, i.e., straightforwardly solving the set of differential equations (1)-(4). The analytical time-evolution dynamics of a single-site initial excitation is exemplified in the eight-site 1D non-Hermitian lattice shown in Fig. 1(a).

Each dimer has a reciprocal coupling  $J$ . The asymmetric couplings with opposite orientations connect every two nearest neighbor dimers; the asymmetric inter dimer coupling strengths are  $\mu = (\kappa - \gamma)/2$  and  $\nu = (\kappa + \gamma)/2$ . The primary resonators have extra gain and loss  $\pm i\Gamma$ . At the EP  $\gamma = \kappa$ , the asymmetric couplings are unidirectional. Any excitation in the red dimer is confined there without escaping because the outward couplings ( $\mu = 0$ ) in magenta vanish and the red dimers only possess inward intercell unidirectional couplings. In contrast, any excitation in the orange cell tunnels to the two neighbor red dimers due to the nonvanishing outward couplings ( $\nu = \kappa$ ) in green, and then the excitation is confined in the two neighbor red dimers.

Applying the Fourier transformation, we obtain the energy bands of the lattice  $E(k) = \pm\sqrt{J^2 - \Gamma^2 + \mu\nu \pm 2J\sqrt{\mu\nu} \cos(k/2)}$ , where the momentum is  $k = 2\pi n/N$  and  $n \in [1, N]$ . The spectra of the photonic resonator lattice for  $\Gamma = 0$  and  $1/2$  are presented in Figs. 1(b) and 1(c). The black hollow circles mark two flat bands; all the levels are two-state coalesced at  $\pm\sqrt{J^2 - \Gamma^2}$ , forming the non-Hermitian AB cage with two coalesced flat bands and resulting in the complete confinement of light excitations. The non-Hermitian AB caging at a high-order EP of four-state coalescence [75] appears when the  $\mathcal{PT}$ -symmetric non-Hermitian dimers are at their own EP ( $J = \Gamma$ ) in addition to the unidirectional inter cell coupling ( $\gamma = \kappa$ ); where all the bands coalesce to a zero-energy flat band as depicted in Fig. 1(d).

The lattice Hamiltonian at the EP is defective, each two-state coalesced eigenstate is associated with a generalized eigenstate [76]. The intensity of initial excitation including eigenstates with different eigenvalues experiences an oscillation [77, 78]; and that including the generalized eigenstate quadratically increases with time [79, 80]. The localized excitation in the non-Hermitian flat band can increase polynomially as a result of the unique dynamics at the EP [29, 30]. Figure 2 shows the intensities of different excitations.

The excitation in a red dimer has limited intensity;

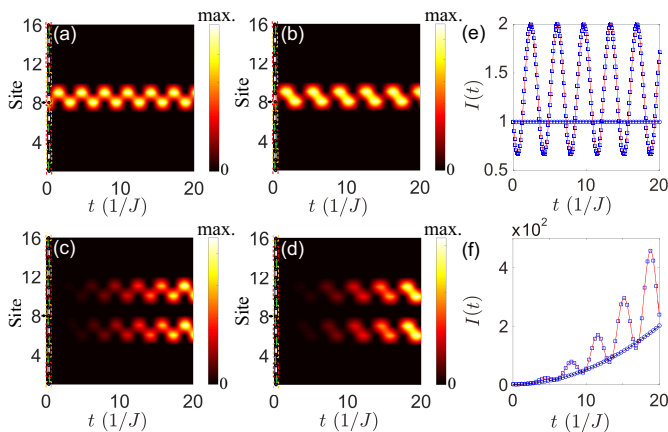


FIG. 2. Non-Hermitian AB caging. Initial excitation is indicated by the yellow arrow in the schematic. The excitation is in (a, b) the red and (c, d) the orange cells. (e) The constant (blue circle) and oscillating (blue square) intensities are depicted for the excitation in the red cell for (a) and (b). (f) The polynomially increasing intensities for the excitations in the orange cell of (c) and (d) are depicted by the blue circle and blue square, respectively.  $\Gamma = 0$  in (a, c) and  $\Gamma = 1/2$  in (b, d); other parameters are  $J = \kappa = \gamma = 1$ . The analytical intensities are indicated by the red and black lines.

whereas the excitation in an orange dimer has quadratically increasing intensity and is confined in its two red neighbor dimers. The excitation on site 8 (9) cannot tunnel leftward (rightward) to site 7 (10). The excitation on site 8 in Fig. 2(a) [Fig. 2(b)] is relevant to the orthogonal (nonorthogonal) eigenstates of the Hermitian (non-Hermitian) lattice; the confined excitation inside the red dimer of sites 8 and 9 has constant (oscillating) intensity [81], which is represented by the blue circles (squares) in Fig. 2(e). The non-Hermiticity results in the nonunitary time evolution; the superposition of eigenvectors with different energies results in the oscillation. By contrast, any excitation in the orange dimer can only tunnel to its two neighbor red dimers, the excitations cannot tunnel backward and then are confined there [Figs. 2(c) and 2(d)]. The excitation in Fig. 2(c) [Fig. 2(d)] is relevant to the generalized eigenstates, which lead to a linear time-dependent excitation amplitude [79]; the excitation intensity increases quadratically over time as presented in Fig. 2(f) by the blue circles (squares). For the non-Hermitian AB caging at the high-order EP, the excitation intensity increases more rapidly [82].

*Destructive interference induced AB cage.*—Synthetic magnetic field for photons has been realized and boosts the study of topological photonics [83–92], particularly in photonic crystals of coupled resonators [69, 93, 94] and waveguides [95, 96]. The Peierls phase induced by the dynamic modulation [95–98] or path length imbalance method in photonics [69, 93] generates the synthetic magnetic flux, which helps the realization of an AB cage in the Hermitian rhombic lattice [35–39].

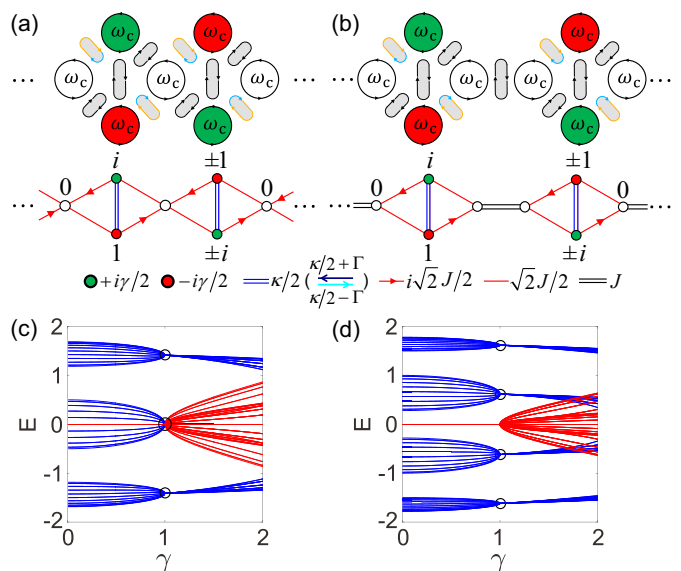


FIG. 3. (a, b) Schematic of the quasi-1D non-Hermitian rhombic lattices under inversion symmetry ( $\Gamma = 0$ ). Each triangular area has a  $\pi/2$  synthetic magnetic flux as a consequence of the Peierls phase induced by the optical length imbalance indicated in the orange and cyan arrows [69]. (c) [(d)] Spectrum of 60 (80) sites for (a) [(b)], the real (imaginary) part is in blue (red). The parameters are  $\Gamma = 0$ ,  $J = \kappa = \gamma = 1$ . The non-Hermitian AB cages of three and four flat bands appear at the EP  $\gamma = 1$ .

The non-Hermitian AB cage under the synthetic magnetic flux is based on another confinement mechanism of the destructive interference. In Fig. 1(e), the nonreciprocal coupling  $\pm iJ/2$  has a Peierls phase factor  $e^{\pm i\pi/2}$ , which leads to a  $\pi$  magnetic flux in each plaquette of the cross-stitch lattice. The destructive interference results in the CLSs localized in a single plaquette and the wavefunctions for the coalesced flat band energies  $\pm J$  are marked in the lower panel. In the discrete Schrödinger equations, the nonreciprocal coupling and the cross-stitch coupling multiplying the wavefunctions  $(1, i)^T$  cancel at the top-left site  $(-iJ/2) \cdot (1) + (J/2) \cdot (i) = 0$  and at the bottom-left site  $(J/2) \cdot (1) + (iJ/2) \cdot (i) = 0$ ; similarly, the interferences of the wavefunctions at the top-right and bottom-right sites are fully destructive. The destructive interference results in zeros for the wavefunction outside the plaquette indicated by the black dashed square.

The synthetic magnetic field associated with balanced gain and loss relates to the asymmetric coupling. Applying a unitary transformation to the  $4N$ -size 1D non-Hermitian lattice in Fig. 1(a), we obtain the quasi-1D non-Hermitian cross-stitch lattice in Fig. 1(e). The dynamics of the non-Hermitian cross-stitch lattice is straightforwardly obtained from the dynamics of the 1D non-Hermitian lattice through the unitary transformation.

The oppositely oriented unidirectional couplings can

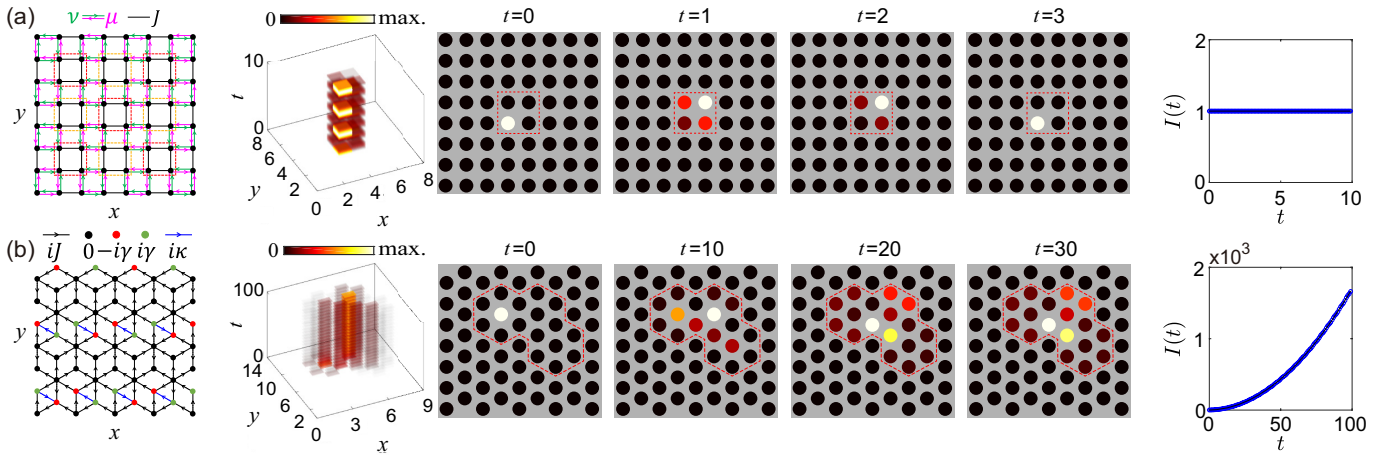


FIG. 4. Non-Hermitian AB caging in the 2D non-Hermitian (a) square lattice and (b) dice lattice. The panels from the left to the right are the lattice schematics, the excitation intensity distribution, and the total excitation intensity for a single-site excitation. Light field is confined inside the dashed red polygon. The parameters are (a)  $J = 1$ ,  $\mu = 0$ ,  $\nu = 1$ ; (b)  $J = 1$ ,  $\kappa = \gamma = 2$ .

form non-Hermitian AB cages consisting of multiple flat bands if we consider oligomer cells instead of dimer cells in Fig. 1(a). The quasi-1D non-Hermitian rhombic lattices with synthetic magnetic flux and balanced gain and loss illustrated in Figs. 3(a) and 3(b) can be obtained similarly under the unitary transformation applied to the connecting sites associated with the unidirectional couplings; the corresponding energy bands are shown in Figs. 3(c) and 3(d), where the non-Hermitian AB caging appears at the EP  $\gamma = \kappa$ .

The Hermitian rhombic lattice in Fig. 3(a) at  $\gamma = \kappa = 0$  is experimentally realized in the coupled optical waveguides [36, 37]. Alternatively introducing  $\mathcal{PT}$ -symmetric dimers at the EP in the rhombic lattices forms the non-Hermitian AB cages [Figs. 3(a) and 3(b)]. The eigenstate of the  $\mathcal{PT}$ -symmetric dimer at the EP  $\gamma = \kappa$  is  $(i, 1)^T$ , the contributions of the extra non-Hermiticity  $\gamma$  and the coupling  $\kappa$  in the discrete Schrödinger equations cancel for the site with gain  $(\kappa/2) \cdot (1) + (i\gamma/2) \cdot (i) = 0$  and for the site with loss  $(\kappa/2) \cdot (i) + (-i\gamma/2) \cdot (1) = 0$ . Thus, the flat band energies and the eigenstates are unchanged in the presence of  $\mathcal{PT}$ -symmetric dimers at the EP, but become coalesced energy levels and coalesced CLSs.

The lower panel of Fig. 3(a) illustrates the cage solutions of the non-Hermitian rhombic lattice. The flat band energy is  $0 (\pm\sqrt{2}J)$ , the corresponding CLS amplitude of the unmarked hollow circle in the center is  $0 (\pm 2i)$ . The wavefunctions of the left (right) dimer destructively interferes at the left (right) site, resulting in the marked zeros. When the symmetric coupling  $\kappa/2$  becomes asymmetric coupling  $\kappa/2 \pm \Gamma$ , all six bands coalesced to a single zero-energy flat band at  $\Gamma = \sqrt{2}J$ .

*Non-Hermitian AB cages in 2D.*—The generality of the two confinement mechanisms is further elucidated through the proposed 2D non-Hermitian AB cages. Fig-

ure 4(a) is the schematic of the non-Hermitian square lattice that exploits the unidirectional coupling to realize the light confinement. Figure 4(b) is the schematic of the non-Hermitian dice lattice that supports the light confinement through the destructive interference under the appropriate match between synthetic magnetic flux and non-Hermiticity.

At the EP  $\mu = 0$  of the non-Hermitian square lattice, all the bands are flat and the energies are  $0, \pm 2J$ . The excitations are confined inside the red plaquette with four symmetric couplings  $J$  in black. The flow of light enters the red plaquette unidirectionally as a consequence that the inter-plaquette couplings of the red plaquettes are inward. Photons tunnel to the red plaquettes without escaping. For any excitation in the orange plaquette, photons tunnel to their neighbor red plaquettes and are confined there.

In the absence of the non-Hermiticity  $\pm i\gamma$  and the non-reciprocal coupling  $i\kappa$ , Fig. 4(b) reduces to the Hermitian dice lattice, which is also referred to as the  $\mathcal{T}_3$  lattice [33]. The synthetic magnetic flux in every diamond plaquette of the dice lattice is  $\pi$  and the destructive interference results in the AB caging with all bands flat at energies  $0, \pm\sqrt{6}J$ . The synthetic magnetic flux  $\pi$  in each diamond plaquette is separated by  $i\kappa$  into two  $+\pi/2$  or  $-\pi/2$  in the triangular areas. The synthetic magnetic fluxes associated with the gain and loss maintains the destructive interference; the eigenvalues and the eigenstates of the Hermitian dice lattice are unchanged after introducing the  $\mathcal{PT}$ -symmetric dimers at the EP  $\gamma = \kappa$ . The contributions of the  $\mathcal{PT}$ -symmetric dimers cancel in the discrete Schrödinger equations of the dice lattice. Arbitrary local light excitation is entirely confined. Notably, the non-Hermitian generalization is nontrivial, we emphasize that although the CLSs are *unchanged* by the

non-Hermiticity; the localization of excitation *changes* due to the CLSs coalescence and the EP unidirectionality [80]. For comparison, the excitation localizes in single snowflake in the Hermitian dice lattice.

The dynamics of a single-site initial excitation in the 2D non-Hermitian AB cages is simulated and presented in the middle panels of Fig. 4. The initial excitation is localized in the plaquette of the non-Hermitian square lattice [Fig. 4(a)] and localized in the three hexagonal area because the snowflake shape CLSs for the non-Hermitian dice lattice [Fig. 4(b)]. The single-site excitation in Fig. 4(b) relates to the generalized eigenstate of the system at the EP; consequently, the excitation probability polynomially increases with time.

*Conclusion.*—We have proposed non-Hermitian AB cages in 1D and 2D at the EP and demonstrated two confinement mechanisms. (i) The unidirectional couplings imposed the inversion (combined-inversion) symmetry. (ii) The destructive interference at the interplay between the gain and loss, the Peierls phase, and the couplings. In both mechanisms, the additional non-Hermitian elements at the EP retain the eigenstates localization; any light excitation not limited to the eigenstate of the non-Hermitian AB cage is completely confined. However, the spectrum of the non-Hermitian AB cage becomes fully constituted by the coalesced flat bands; and the localized area of excitation may alter and affected by the EP unidirectionality. The non-Hermiticity induces the nonunitary dynamics. The intensity may periodically oscillate or polynomially increase. The non-Hermitian AB cages proposed in the photonic resonator lattices can be implemented in the coupled waveguides as well [28, 36].

In addition, offsetting an overall imaginary energy  $i\gamma$  in the passive system with losses 0 and  $-2i\gamma$  yields the active  $\mathcal{PT}$ -symmetric lattice with balanced gain and loss  $\pm i\gamma$  [28, 63–66, 99]; the non-Hermitian AB cages are possible to be realized in passive photonic lattice through judiciously engineering losses of the sublattices. Recent progresses on the Hermitian AB cage [36], the non-Hermitian flat band [28], and the  $\mathcal{PT}$ -symmetric photonic crystal [66, 99] indicate the non-Hermitian AB cages proposed are experimentally accessible.

*Acknowledgement.*—We acknowledge the support from National Natural Science Foundation of China under Grant No. 11975128.

---

\* jinliang@nankai.edu.cn

- [1] C. E. Creffield and G. Platero, Coherent Control of Interacting Particles Using Dynamical and Aharonov-Bohm Phases, *Phys. Rev. Lett.* **105**, 086804 (2010).
- [2] N. Masumoto, N. Y. Kim, T. Byrnes, K. Kusudo, A. Löffler, S. Höfling, A. Forchel, and Y. Yamamoto, Exciton-polariton condensates with flat bands in a two-dimensional kagome lattice, *New J. Phys.* **14**, 065002 (2012).
- [3] D. Leykam, O. Bahat-Treidel, and A. S. Desyatnikov, Flat band states: Disorder and nonlinearity, *Phys. Rev. B* **88**, 224203 (2013); S. Flach, D. Leykam, J. D. Bodyfelt, P. Matthies, and A. S. Desyatnikov, Detangling flat bands into Fano lattices, *Eur. Phys. Lett.* **105**, 30001 (2014).
- [4] J. D. Bodyfelt, D. Leykam, C. Danieli, X. Yu, and S. Flach, Flatbands under Correlated Perturbations, *Phys. Rev. Lett.* **113**, 236403 (2014).
- [5] T. Jacqmin, I. Carusotto, I. Sagnes, M. Abbarchi, D. D. Solnyshkov, G. Malpuech, E. Galopin, A. Lemaître, J. Bloch, and A. Amo, Direct Observation of Dirac Cones and a Flatband in a Honeycomb Lattice for Polaritons, *Phys. Rev. Lett.* **112**, 116402 (2014).
- [6] R. Khomeriki and S. Flach, Landau-Zener Bloch Oscillations with Perturbed Flat Bands, *Phys. Rev. Lett.* **116**, 245301 (2016).
- [7] L. Morales-Inostroza and R. A. Vicencio, Simple method to construct flat-band lattices, *Phys. Rev. A* **94**, 043831 (2016).
- [8] F. Baboux, L. Ge, T. Jacqmin, M. Biondi, E. Galopin, A. Lemaître, L. Le Gratiet, I. Sagnes, S. Schmidt, H. E. Türeci, A. Amo, and J. Bloch, Bosonic Condensation and Disorder-Induced Localization in a Flat Band, *Phys. Rev. Lett.* **116**, 066402 (2016).
- [9] A. Ramachandran, A. Andreanov, and S. Flach, Chiral flat bands: Existence, engineering, and stability, *Phys. Rev. B* **96**, 161104(R) (2017); W. Maimaiti, A. Andreanov, H. C. Park, O. Gendelman, and S. Flach, Compact localized states and flat-band generators in one dimension, *Phys. Rev. B* **95**, 115135 (2017).
- [10] M. Tovmasyan, S. Peotta, L. Liang, P. Törmä, and S. D. Huber, Preformed pairs in flat Bloch bands, *Phys. Rev. B* **98**, 134513 (2018).
- [11] D. Leykam, A. Andreanov, and S. Flach, Artificial flat band systems: from lattice models to experiments, *Adv. Phys. X* **3**, 1473052 (2018).
- [12] D. Guzmán-Silva, C. Mejía-Cortés, M. A. Bandres, M. C. Rechtsman, S. Weimann, S. Nolte, M. Segev, A. Szameit, and R. A. Vicencio, Experimental observation of bulk and edge transport in photonic Lieb lattices, *New J. Phys.* **16**, 063061 (2014).
- [13] S. Mukherjee and R. R. Thomson, Observation of localized flat-band modes in a quasi-one-dimensional photonic rhombic lattice, *Opt. Lett.* **40**, 5443 (2015).
- [14] R. A. Vicencio, C. Cantillano, L. Morales-Inostroza, B. Real, C. Mejía-Cortés, S. Weimann, A. Szameit, and M. I. Molina, Observation of Localized States in Lieb Photonic Lattices, *Phys. Rev. Lett.* **114**, 245503 (2015).
- [15] S. Mukherjee, A. Spracklen, D. Choudhury, N. Goldman, P. Öhberg, E. Andersson, and R. R. Thomson, Observation of a Localized Flat-Band State in a Photonic Lieb Lattice, *Phys. Rev. Lett.* **114**, 245504 (2015).
- [16] S. Mukherjee and R. R. Thomson, Observation of robust flat-band localization in driven photonic rhombic lattices, *Opt. Lett.* **42**, 2243 (2017).
- [17] S. Longhi, Parity-time symmetry meets photonics: A new twist in non-Hermitian optics, *Europhys. Lett.* **120**, 64001 (2017).
- [18] L. Feng, R. El-Ganainy, and L. Ge, Non-Hermitian photonics based on parity-time symmetry, *Nat. Photon.* **11**, 752 (2017).

- [19] G. Gbur and K. Makris, Introduction to non-Hermitian photonics in complex media:  $\mathcal{PT}$ -symmetry and beyond, *Photon. Res.* **6**, PTS1 (2018).
- [20] R. El-Ganainy, K. G. Makris, M. Khajavikhan, Z. H. Musslimani, S. Rotter, and D. N. Christodoulides, Non-Hermitian physics and  $\mathcal{PT}$  symmetry, *Nat. Phys.* **14**, 11 (2018).
- [21] S. K. Gupta, Y. Zou, X.-Y. Zhu, M.-H. Lu, L. Zhang, X.-P. Liu, and Y.-F. Chen, Parity-time symmetry in non-Hermitian complex media, *Adv. Mater.* 1903639 (2019).
- [22] D. Christodoulides and J. Yang, *Parity-Time Symmetry and Its Applications* (Springer, Berlin, 2018).
- [23] S. K. Özdemir, S. Rotter, F. Nori, and L. Yang, Parity-time symmetry and exceptional points in photonics, *Nat. Mater.* **18**, 783 (2019).
- [24] M. A. Miri and A. Alù, Exceptional points in optics and photonics, *Science* **363**, eaar7709 (2019).
- [25] M. I. Molina, Flat bands and  $\mathcal{PT}$  symmetry in quasi-one-dimensional lattices, *Phys. Rev. A* **92**, 063813 (2015).
- [26] L. Ge, Parity-time symmetry in a flat-band system, *Phys. Rev. A* **92**, 052103 (2015).
- [27] H. Ramezani, Non-Hermiticity-induced flat band, *Phys. Rev. A* **96**, 011802(R) (2017).
- [28] T. Biesenha, M. Kremer, M. Heinrich, and A. Szameit, Experimental Realization of  $\mathcal{PT}$ -Symmetric Flat Bands, *Phys. Rev. Lett.* **123**, 183601 (2019).
- [29] D. Leykam, S. Flach, and Y. D. Chong, Flat bands in lattices with non-Hermitian coupling, *Phys. Rev. B* **96**, 064305 (2017).
- [30] L. Ge, Non-Hermitian lattices with a flat band and polynomial power increase, *Photon. Res.* **6**, A10 (2018).
- [31] B. Qi, L. Zhang, and L. Ge, Defect States Emerging from a Non-Hermitian Flatband of Photonic Zero Modes, *Phys. Rev. Lett.* **120**, 093901 (2018).
- [32] L. Jin, Flat band induced by the interplay of synthetic magnetic flux and non-Hermiticity, *Phys. Rev. A* **99**, 033810 (2019); S. M. Zhang and L. Jin, Flat band in two-dimensional non-Hermitian optical lattices, *Phys. Rev. A* **100**, 043808 (2019).
- [33] J. Vidal, R. Mosseri, and B. Douçot, Aharonov-Bohm Cages in Two-Dimensional Structures, *Phys. Rev. Lett.* **81**, 5888 (1998).
- [34] J. Vidal, P. Butaud, B. Douçot, and R. Mosseri, Disorder and interactions in Aharonov-Bohm cages, *Phys. Rev. B* **64**, 155306 (2001).
- [35] S. Longhi, Aharonov–Bohm photonic cages in waveguide and coupled resonator lattices by synthetic magnetic fields, *Opt. Lett.* **39**, 5892 (2014).
- [36] S. Mukherjee, M. Di Liberto, P. Öhberg, R. R. Thomson, and N. Goldman, Experimental Observation of Aharonov-Bohm Cages in Photonic Lattices, *Phys. Rev. Lett.* **121**, 075502 (2018).
- [37] M. Kremer, I. Petrides, E. Meyer, M. Heinrich, O. Zilberberg, and A. Szameit, Non-quantized square-root topological insulators: a realization in photonic Aharonov-Bohm cages, arXiv:1805.05209.
- [38] G. Gligorić, P. P. Belićev, D. Leykam, and A. Maluckov, Nonlinear symmetry breaking of Aharonov-Bohm cages, *Phys. Rev. A* **99**, 013826 (2019).
- [39] M. Di Liberto, S. Mukherjee, and N. Goldman, Nonlinear dynamics of Aharonov-Bohm cages, *Phys. Rev. A* **100**, 043829 (2019).
- [40] J. Wiersig, Enhancing the Sensitivity of Frequency and Energy Splitting Detection by Using Exceptional Points: Application to Microcavity Sensors for Single-Particle Detection, *Phys. Rev. Lett.* **112**, 203901 (2014).
- [41] M. Am-Shallem, R. Kosloff and N. Moiseyev, Exceptional points for parameter estimation in open quantum systems: analysis of the Bloch equations, *New J. Phys.* **17**, 113036 (2015).
- [42] Z.-P. Liu, J. Zhang, S. K. Özdemir, B. Peng, H. Jing, X.-Y. Lü, C.-W. Li, L. Yang, F. Nori, and Y. X. Liu, Metrology with  $\mathcal{PT}$ -Symmetric Cavities: Enhanced Sensitivity near the  $\mathcal{PT}$ -Phase Transition, *Phys. Rev. Lett.* **117**, 110802 (2016).
- [43] H. Hodaie, A. U. Hassan, S. Wittek, H. Garcia-Gracia, R. El-Ganainy, D. N. Christodoulides, and M. Khajavikhan, Enhanced sensitivity at higher-order exceptional points, *Nature (London)* **548**, 187 (2017).
- [44] W. Chen, S. K. Özdemir, G. Zhao, J. Wiersig, and L. Yang, Exceptional points enhance sensing in an optical microcavity, *Nature (London)* **548**, 192 (2017).
- [45] H.-K. Lau and A. A. Clerk, Fundamental limits and non-reciprocal approaches in non-Hermitian quantum sensing, *Nat. Commun.* **9**, 4320 (2018).
- [46] W. Chen, J. Zhang, B. Peng, S. K. Özdemir, X. Fan, and L. Yang, Parity-time-symmetric whispering-gallery mode nanoparticle sensor, *Photon. Res.*, **6**, 05000A23 (2018).
- [47] M. Zhang, W. Sweeney, C. W. Hsu, L. Yang, A. D. Stone, and L. Jiang, Quantum Noise Theory of Exceptional Point Sensors, *Phys. Rev. Lett.* **123**, 180501 (2019).
- [48] C. Chen, L. Jin, and R.-B. Liu, Sensitivity of parameter estimation near the exceptional point of a non-Hermitian system, *New J. Phys.* **21**, 083002 (2019).
- [49] P. Djourwe, Y. Pennec, and B. Djafari-Rouhani, Exceptional Point Enhances Sensitivity of Optomechanical Mass Sensors, *Phys. Rev. Applied* **12**, 024002 (2019).
- [50] Y.-H. Lai, Y.-K. Lu, M.-G. Suh, Z. Yuan, and K. Vahala, Observation of the exceptional-point-enhanced Sagnac effect, *Nature* **576**, 65 (2019).
- [51] M. P. Hokmabadi, A. Schumer, D. N. Christodoulides, and M. Khajavikhan, Non-Hermitian ring laser gyroscopes with enhanced Sagnac sensitivity, *Nature* **576**, 70 (2019).
- [52] H. Xu, D. Mason, L. Jiang, and J. G. E. Harris, Topological energy transfer in an optomechanical system with exceptional points, *Nature (London)* **537**, 80 (2016).
- [53] S. Assaworarith, X. Yu, and S. Fan, Robust wireless power transfer using a nonlinear parity-time-symmetric circuit, *Nature (London)* **546**, 387 (2017).
- [54] H. Ramezani, H.-K. Li, Y. Wang, and X. Zhang, Unidirectional Spectral Singularities, *Phys. Rev. Lett.* **113**, 263905 (2014).
- [55] B. Peng, S. K. Özdemir, M. Liertzer, W. Chen, J. Kramer, H. Yılmaz, J. Wiersig, S. Rotter, and L. Yang, Chiral modes and directional lasing at exceptional points, *Proc. Natl. Acad. Sci. U.S.A.* **113**, 6845 (2016).
- [56] L. Jin and Z. Song, Incident Direction Independent Wave Propagation and Unidirectional Lasing, *Phys. Rev. Lett.* **121**, 073901 (2018).
- [57] D. L. Sounas and A. Alù, Non-reciprocal photonics based on time modulation, *Nat. Photon.* **11**, 774 (2017).
- [58] M.-A. Miri, F. Ruesink, E. Verhagen, and A. Alù, Optical Nonreciprocity Based on Optomechanical Coupling, *Phys. Rev. Applied* **7**, 064014 (2017).
- [59] L. Fan, J. Wang, L. T. Varghese, H. Shen, B. Niu, Y.

- Xuan, A. M. Weiner, and M. Qi, An all-silicon passive optical diode, *Science* **335**, 447 (2012).
- [60] P. St-Jean, V. Goblot, E. Galopin, A. Lemaitre, T. Ozawa, L. Le Gratiet, I. Sagnes, J. Bloch, and A. Amo, Lasing in topological edge states of a one-dimensional lattice, *Nat. Photon.* **11**, 651 (2017).
- [61] M. Parto, S. Wittek, H. Hodaie, G. Harari, M. A. Bandres, J. Ren, M. C. Rechtsman, M. Segev, D. N. Christodoulides, and M. Khajavikhan, Edge-mode lasing in 1D topological active arrays, *Phys. Rev. Lett.* **120**, 113901 (2018).
- [62] H. Zhao, P. Miao, M. H. Teimourpour, S. Malzard, R. El-Ganainy, H. Schomerus, and L. Feng, Topological hybrid silicon microlasers, *Nat. Commun.* **9**, 981 (2018).
- [63] C. Poli, M. Bellec, U. Kuhl, F. Mortessagne, and H. Schomerus, Selective enhancement of topologically induced interface states in a dielectric resonator chain, *Nat. Commun.* **6**, 6710 (2015).
- [64] S. Weimann, M. Kremer, Y. Plotnik, Y. Lumer, S. Nolte, K. G. Makris, M. Segev, M. C. Rechtsman, and A. Szameit, Topologically protected bound states in photonic parity-time-symmetric crystals, *Nat. Mater.* **16**, 433 (2017).
- [65] M. Pan, H. Zhao, P. Miao, S. Longhi, and L. Feng, Photonic zero mode in a non-Hermitian photonic lattice, *Nat. Commun.* **9**, 1308 (2018).
- [66] A. Cerjan, S. Huang, K. P. Chen, Y. Chong, and M. C. Rechtsman, Experimental realization of a Weyl exceptional ring, *Nat. Photon.* **13**, 623 (2019).
- [67] S. Longhi, D. Gatti and G. Della Valle, Robust light transport in non-Hermitian photonic lattices, *Sci. Rep.* **5**, 13376 (2015); Non-Hermitian transparency and one-way transport in low-dimensional lattices by an imaginary gauge field, *Phys. Rev. B* **92**, 094204 (2015).
- [68] D. Jalas, A. Petrov, M. Eich, W. Freude, S. Fan, Z. Yu, R. Baets, M. Popović, A. Melloni, J. D. Joannopoulos, M. Vanwolleghem, C. R. Doerr, and H. Renner, What is and what is not an optical isolator, *Nat. Photon.* **7**, 579 (2013).
- [69] M. Hafezi, Synthetic gauge fields with photons, *Int. J. Mod. Phys. B* **28**, 1441002 (2014); M. Hafezi, Measuring Topological Invariants in Photonic Systems, *Phys. Rev. Lett.* **112**, 210405 (2014).
- [70] N. Hatano and D. R. Nelson, Localization Transitions in Non-Hermitian Quantum Mechanics, *Phys. Rev. Lett.* **77**, 570 (1996).
- [71] X. Z. Zhang and Z. Song, Momentum-independent reflectionless transmission in the non-Hermitian time-reversal symmetric system, *Ann. Phys. (NY)* **339**, 109 (2013).
- [72] B. Midya, H. Zhao, and L. Feng, Non-Hermitian photonics promises exceptional topology of light, *Nat. Commun.* **9**, 2674 (2018).
- [73] L. Jin and Z. Song, Bulk-boundary correspondence in a non-Hermitian system in one dimension with chiral inversion symmetry, *Phys. Rev. B* **99**, 081103(R) (2019).
- [74] J. D. Joannopoulos, S. G. Johnson, J. N. Winn, and R. D. Meade, *Photonic Crystals: Modeling the Flow of Light* (Princeton University Press, Princeton, NJ, 2008).
- [75] L. Jin, Parity-time-symmetric coupled asymmetric dimers, *Phys. Rev. A* **97**, 012121 (2018).
- [76] G. Golub and C. F. van Loan, *Matrix Computations* (Johns Hopkins University Press, Baltimore, 1996).
- [77] C. E. Rüter, K. G. Makris, R. El-Ganainy, D. N. Christodoulides, M. Segev, and D. Kip, Observation of parity-time symmetry in optics, *Nat. Phys.* **6**, 192 (2010).
- [78] L. Jin and Z. Song, Hermitian dynamics in a class of pseudo-Hermitian networks, *Phys. Rev. A* **84**, 042116 (2011).
- [79] P. Wang, L. Jin, G. Zhang, and Z. Song, Wave emission and absorption at spectral singularities, *Phys. Rev. A* **94**, 053834 (2016).
- [80] C. Li, L. Jin, and Z. Song, Non-Hermitian interferometer: Unidirectional amplification without distortion, *Phys. Rev. A* **95**, 022125 (2017).
- [81] L. Jin and Z. Song, Hermitian dynamics in a class of pseudo-Hermitian networks, *Phys. Rev. A* **84**, 042116 (2011).
- [82] Q. Zhong, D. N. Christodoulides, M. Khajavikhan, K. G. Makris, and R. El-Ganainy, Power-law scaling of extreme dynamics near higher-order exceptional points, *Phys. Rev. A* **97**, 020105(R) (2018).
- [83] N. Goldman, G. Juzeliūnas, P. Öhberg and I. B. Spielman, Light-induced gauge fields for ultracold atoms, *Rep. Prog. Phys.* **77**, 126401 (2014).
- [84] N. Goldman, J. C. Budich, and P. Zoller, Topological quantum matter with ultracold gases in optical lattices, *Nat. Phys.* **12**, 639 (2016).
- [85] I. Bloch, J. Dalibard, and S. Nascimbène, Quantum simulations with ultracold quantum gases, *Nat. Phys.* **8**, 267 (2012); C. Gross and I. Bloch, Quantum simulations with ultracold atoms in optical lattices, *Science* **357**, 995 (2017).
- [86] D.-W. Zhang, Y.-Q. Zhu, Y. X. Zhao, H. Yan, and S.-L. Zhu, Topological quantum matter with cold atoms, *Adv. Phys.* **67**, 253 (2019).
- [87] N. R. Cooper, J. Dalibard, and I. B. Spielman, Topological bands for ultracold atoms, *Rev. Mod. Phys.* **91**, 015005 (2019).
- [88] L. Lu, J. D. Joannopoulos, and M. Soljačić, Topological photonics, *Nat. Photon.* **8**, 821 (2014); Topological states in photonic systems, *Nat. Phys.* **12**, 626 (2016).
- [89] T. Ozawa, H. M. Price, A. Amo, N. Goldman, M. Hafezi, L. Lu, M. Rechtsman, D. Schuster, J. Simon, O. Zilberberg, and I. Carusotto, Topological photonics, *Rev. Mod. Phys.* **91**, 015006 (2019).
- [90] M. Xiao, W.-J. Chen, W.-Y. He, and C. T. Chan, Synthetic gauge flux and Weyl points in acoustic systems, *Nat. Phys.* **11**, 920 (2015).
- [91] Z. Yang, F. Gao, X. Shi, X. Lin, Z. Gao, Y. Chong, and B. Zhang, Topological Acoustics, *Phys. Rev. Lett.* **114**, 114301 (2015).
- [92] M. C. Rechtsman, J. M. Zeuner, Y. Plotnik, Y. Lumer, D. Podolsky, F. Dreisow, S. Nolte, M. Segev, and A. Szameit, Photonic Floquet topological insulators, *Nature* **496**, 196 (2013).
- [93] M. Hafezi, E. A. Demler, M. D. Lukin, and J. M. Taylor, Robust optical delay lines with topological protection, *Nat. Phys.* **7**, 907 (2011).
- [94] Q. Lin and S. Fan, Light Guiding by Effective Gauge Field for Photons, *Phys. Rev. X* **4**, 031031 (2014).
- [95] Z. Yu and S. Fan, Complete optical isolation created by indirect interband photonic transitions, *Nat. Photon.* **3**, 91 (2009).
- [96] K. Fang, Z. Yu, and S. Fan, Photonic Aharonov-Bohm Effect Based on Dynamic Modulation, *Phys. Rev. Lett.* **108**, 153901 (2012); K. Fang, Z. Yu, and S. Fan, Real-

- izing effective magnetic field for photons by controlling the phase of dynamic modulation, *Nat. Photon.* **6**, 782 (2012).
- [97] N. Goldman and J. Dalibard, Periodically Driven Quantum Systems: Effective Hamiltonians and Engineered Gauge Fields, *Phys. Rev. X* **4**, 031027 (2014).
- [98] P. Roushan, C. Neill, A. Megrant, Y. Chen, R. Babush, R. Barends, B. Campbell, Z. Chen, B. Chiaro, A. Dunsworth, A. Fowler, E. Jeffrey, J. Kelly, E. Lucero, J. Mutus, P. J. J. O'Malley, M. Neeley, C. Quintana, D. Sank, A. Vainsencher, J. Wenner, T. White, E. Kapit, H. Neven, and J. Martinis, Chiral ground-state currents of interacting photons in a synthetic magnetic field, *Nat. Phys.* **13**, 146 (2017).
- [99] M. Kremer, T. Biesenthal, L. J. Maczewsky, M. Heinrich, R. Thomale, and A. Szameit, Demonstration of a two-dimensional  $\mathcal{PT}$ -symmetric crystal, *Nat. Commun.* **10**, 435 (2019).